Journal of Intelligent & Robotic Systems (2020) 98:525–538
https://doi.org/10.1007/s10846-019-01063-5

Influence of a Compatible Design on Physical Human-Robot Interaction Force: a Case Study of a Self-Adapting Lower-Limb Exoskeleton Mechanism

Jianfeng Li[1] · Shiping Zuo[1] · Chenghui Xu[1] · Leiyu Zhang[1] · Mingjie Dong[1] · Chunjing Tao[2] · Run Ji[2]

Received: 21 February 2019 / Accepted: 9 July 2019 / Published online: 27 July 2019
© Springer Nature B.V. 2019

Abstract
In the kinematic design of wearable exoskeletons, the issue of axis misalignments between the human and the exoskeleton joints should be well dealt with. Otherwise, large physical human-robot interaction (p-HRI) forces may occur at the human-robot interfaces, which makes the p-HRI uncomfortable or even unsafe. To cope with this issue, a kinematically compatible design approach of wearable exoskeletons has been investigated by researchers, and great development has been made in recent years. Moreover, the influence of such a design on the exoskeleton's p-HRI performance should be evaluated to determine if the design is feasible. In this paper, a self-adapting lower-limb exoskeleton mechanism for three degrees of freedom gait training is proposed, and the mechanical structure of the exoskeleton mechanism is designed in detail. Then, based on the presented exoskeleton mechanism and the use of suitable force/torque sensors, a p-HRI force measurement system is developed. Subsequently, the p-HRI forces of the human-robot closed chain under the static and motion modes are detected, and the influence of the self-adapting design on the lower-limb exoskeleton mechanism's p-HRI force feature is evaluated. The results indicate that additional human-robot connective joints could reduce the p-HRI force significantly, the compatible design of the exoskeleton mechanism is effective, and is thus applied to human lower-limb gait training.

Keywords Lower-limb exoskeleton mechanism · Compatible design · Axis misalignment · Self-adapting · Physical human-robot interaction force

1 Introduction

Throughout the past two decades, various wearable lower-limb exoskeletons (e.g., the Lokomat [1], the ALEX III [2], and the LOPES [3]) have been developed for the rehabilitation treatment of individuals suffering from impaired mobility and gait disorders. Compared with manual-assisted gait training, exoskeleton-assisted gait training features several advantages, including low labor intensiveness, long duration, easy repeatability, and task orientation [4–6]. However, problems in exoskeleton-assisted training emerge as a result of the close physical human–robot interaction (p-HRI) between the exoskeletons and the human lower limbs. Specially, the issue of axis misalignment between the human and the exoskeleton joints must be well dealt with when the exoskeletons are connected to the human bodies. Otherwise, axis misalignment leads to a hyperstaticity of the human-robot closed chains, and uncontrollable hyperstatic forces may occur at the human–robot interfaces [7, 8]. These undesired forces do not contribute to the gait training task and change with the movement of the human-robot closed chains; additionally, the gait training becomes uncomfortable or even unsafe when they are sufficiently large.

An effective approach to coping with the issue of axis misalignment is the compatible design of the wearable exoskeletons, in which additional joints or degrees of freedom (DOFs) are added into the exoskeleton structures (usually simple kinematically bionic chains of the human limbs). These introduced joints ensure that the human-robot closed chains are not hyperstatic anymore and hence decrease the uncontrollable hyperstatic forces. According to the installation locations of the additional joints in exoskeletons and the

✉ Leiyu Zhang
zhangleiyu1988@126.com

[1] College of Mechanical Engineering and Applied Electronics Technology, Beijing University of Technology, Beijing 100124, People's Republic of China

[2] National Research Center for Rehabilitation Technical Aids, Beijing 100176, People's Republic of China

treatment strategy of axis misalignment, such designed exoskeletons could be classified into two categories: self–tracing exoskeletons and self–adapting exoskeletons. In self-tracing exoskeletons, additional joints are introduced into the exoskeletons between the base and the active joints or between two subsequent active joints. These added DOFs allow for the axes of the exoskeleton's active joints to trace those of the human joints during the training process [9–15]. In self-adapting exoskeletons, additional joints are introduced into the exoskeletons to reduce the hyperstatic forces without the necessity of axes–tracing between the exoskeleton's active joint and the human joints [16–23]. Notably, some exoskeletons proposed in [24–27] are designed with no need for axis alignment. Specifically, by using the shadow-leg concept, LOPES II [24] transfers the torques from motor to patient via a mechanical structure of push-pull rods, and realizes minimal amount of clamps, no need for exact joint alignment, small misalignment of the rods, arm swing unhindered, short donning and doffing time. Moreover, by using human as the underlying mechanical structure, cable-driven exoskeletons [25–27] also do not require the joint alignment between the human segments and the robot.

Up to now, various wearable exoskeletons have been developed based on the self–tracing and self–adapting design strategy. For example, in the kinematic design of a nine-DOF upper-limb exoskeleton [7], two passive joints were used to connect the human and the exoskeleton forearms. In the NEUROExos exoskeleton proposed in [12], four passive DOFs were introduced to ensure the axis alignment between the exoskeleton and the human elbow joints. Wu et al. [13] built entire upper-limb exoskeleton on a self-tracing frictionless linear platform to compensate the horizontal human-robot misalignment. Based on biomechanical design, Lee et al. [14] presented a flexible exoskeleton with kinematically similar anthropomorphic joints, in which a self-tracing knee joint consisting of four pulleys was proposed to compensate the misaligned joint axes between the human and robot caused by a bending knee. In LIMPACT exoskeleton proposed by Otten et al. [15], an aligning mechanism consisting of two parallelograms and a four-bar linkage was designed for elbow; two adjustable DOFs are designed for various upper and lower arm lengths and sizes. In the Shoulde-Ro exoskeleton designed for shoulder rehabilitation application [17, 18], the additional joints were linked serially and served as the passive human-robot connective sub-chain to reduce the hyperstatic forces. By adding misalignment compensation joints in the exoskeleton structure proposed by Bartenbach et al. [19], the cuff attachment can slide up and down as a passive prismatic joint along the tubes with minimal resistance, which avoids undesirable force from misalignment. In [20], a self-adapting exoskeleton was designed for flexion/extension assistance of the hip, in which five passive DOFs were introduced to realize the compatible design of the assistive exoskeleton. The general methodology for developing a compatible design of wearable exoskeletons has also been addressed by researchers. In [21], a joint motion decoupling-based method was proposed by mounting the exoskeleton's active joints on passive moveable mechanisms. In [22], a graph-based method for kinematic design of the compatible lower-limb exoskeletons was investigated, and several solutions of axis alignment free exoskeletons were enumerated. Based on rank analyses of the twist and wrench spaces of the human-robot closed chains, a general design method of the self-adapting upper-limb exoskeletons was proposed in [23], which clearly showed the methods about introducing passive DOFs into the exoskeletons to avoid the hyperstaticity of the human-robot closed chains. In [28, 29], the hyperstatic force caused by axis misalignment was analyzed from an over-actuation perspective, and a simple design method of the self-adapting exoskeletons for training applications was proposed, by means of the traditional DOF theory of the spatial multi-loop kinematic chains.

In addition to the solution for the issue of axis misalignment, studies have also paid attention to the p-HRI performance of wearable exoskeletons, particularly the feature of p-HRI force, and two kinds of force measurement approaches have been proposed: load cell-based and pressure sensor-based detections. In the load cell-based method, the p-HRI forces are measured at the attachment points by the load cells placed at the connective interfaces between the cuff/orthosis and the exoskeleton links, such as in the ESA Human Arm Exoskeleton [30], ALEX [31], and MIT leg exoskeleton [32]. In the pressure sensor-based approach, the well-designed sensors or sensor arrays, for example, the soft silicone pressure sensor [33], Interlink Electronics FSR [34], and Pressure Sensor Pads [35], were inserted between the human body and the cuff interfaces, through which the distributed interaction force was measured directly. Despite making significant advancements and developing various sensor measurement systems, the works focus on obtaining an accurate interaction force measurement, more to assess the wearer's reaction to the function assistance than to evaluate the influence of the kinematic design on the exoskeleton's p-HRI performance.

To date, there have been few studies analyzing the p-HRI force characteristics of compatibly designed wearable exoskeletons. Zanotto et al. [36] reported the effects of human-robot misalignment (more precisely, knee joint misalignment) on healthy subject's gait in terms of kinematic, kinetics and gait timing; and evidenced the significant change on p-HRI caused by this misalignment. In [37], a mechanical model describing the causes and effects of axis misalignment between a human elbow joint and an exoskeleton joint was proposed, based on which an analytical model to predict the interactional force caused by misaligned joint axes was established through experimental test and parameter estimation. Following the same research line, the influence of the kinematic configuration, the attachment pressure, and the axis misalignment on exoskeleton's

p-HRI forces was further investigated in [38, 39]. In another related study [40], a four-DOF upper-limb rehabilitation exoskeleton named ABLE was developed, and the p-HRI forces corresponding to ABLE with/without passive human-robot connective joints were detected and compared experimentally. In accordance with the results of the above studies, one can find that wearable exoskeletons with passive connective joints could greatly reduce the p-HRI forces.

In this paper, compared with the previous works, we proposed a novel compatible design (i.e., a self-adapting kinematic configuration which introduces additional joints into the human-robot connections to replace rigid connective parts and reduce undesired interactional loads in the human-robot closed chains) of the lower-limb exoskeleton mechanism for three-DOF gait training. Moreover, to specially evaluate the influence of this self-adapting design concept on the p-HRI performance, a p-HRI force measurement system was developed. Considering the gait mode and the static mode, the p-HRI force was detected, and the force feature was analyzed. The remainder of the paper is organized as follows. In Section 2, a self-adapting kinematic configuration of the lower-limb exoskeleton mechanism is proposed, the structure of the exoskeleton mechanism is designed in detail, and then a p-HRI force measurement system is developed based on the presented exoskeleton mechanism. In Section 3, the p–HRI forces of the human-robot closed chains formed by the exoskeleton mechanism and the human legs, under the static and motion modes, are detected, respectively, based on which the influence of the self-adapting design on the p-HRI force feature is analyzed. Finally, the conclusions are given in Section 4.

2 The P-HRI Force Measurement System of the Lower-Limb Exoskeleton Mechanism

In this section, the kinematic configuration of the self-adapting lower-limb exoskeleton mechanism is proposed, the mobility of the human-robot closed chain generated by human leg and exoskeleton mechanism is analyzed, and the mechanical structure of the exoskeleton mechanism is designed. In particular, the working principle and the detailed structures of the human-robot connective joints equipped with removable sheets and pins are presented, which allow for the wearer to lock/unlock the connective joints quickly without detaching the leg from the exoskeleton mechanism. Finally, the p-HRI force detection system is developed.

2.1 Configuration of the Exoskeleton Mechanism

According to the biological model of the human leg [41], it is known that the head of the femur cannot slide with respect to the cotyle face but can turn in the cotyle freely in the hip joint. Thus, the hip joint possesses three rotational DOFs. A human knee joint also has three rotational DOFs; however, due to the tight constraints of the joint capsule and the crossed ligaments, the AD/AB and IN/EX rotations are very small [42]. Moreover, because of the "loose" attribute [43], in bionics of the knee joint, the knee joint cannot be treated as a traditional hinge joint but as a one-DOF revolute joint with an instantaneous axis [44]. With these considerations, a kinematic model of the human lower-limb can be constructed, as shown in Fig. 1. In this model, the hip joint is regarded as a three–DOF spherical joint, and the knee joint is replaced by a one-DOF four-bar linkage mechanism [45–49], in which the joint's rotation is coupled with the sliding motion of its instantaneous axis. Moreover, in the process of human-robot motion, this instantaneous axis causes a misalignment of joint when using a revolute joint to simulate the knee joint motion in exoskeleton structure, and then may produces undesired interactional load on human (i.e., if the critical problem of axes misalignment is not solved well, the undesired force will be entirely unloaded on human's skin, soft issue and joint).

To date, there have been some lower–limb exoskeletons developed for three-DOF gait training (i.e., the AD/AB and FL/EX DOFs of the hip, as well as the FL/EX DOF of the knee), and the classical ones among them are the LOPES [3] and ALEX [31] exoskeletons, as shown in Figs. 2 and 3, respectively, where the human leg is represented in yellow, exoskeleton mechanism is represented in blue, and additional joints are represented in green. Specifically, three passive prismatic joints and a parallelogram mechanism are added into the exoskeleton kinematic chains between the base and the hip active joints of the LOPES exoskeleton while a one-DOF parallelogram mechanism, a passive prismatic joint and a passive revolute joints are implemented at the same position of the ALEX exoskeleton, to allow for the axes of the exoskeleton's active joints to trace those of the human joints. According to the functions and the install locations of the passive joints, the LOPES and the ALEX could be classified

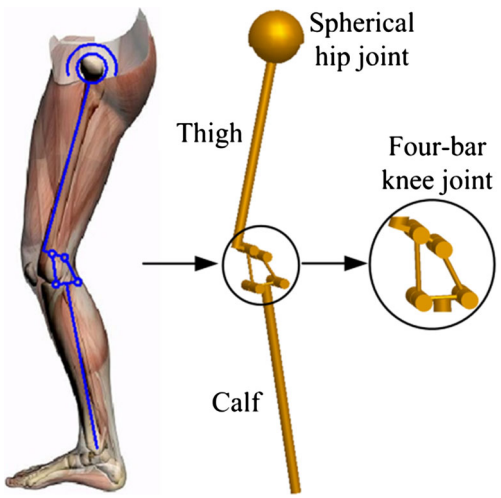

Fig. 1 Kinematic model of the human lower-limb

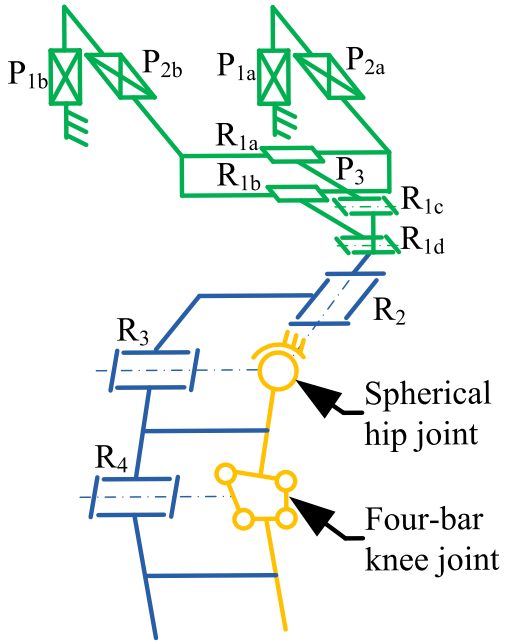

Fig. 2 Kinematic chain of the LOPES exoskeleton [3]

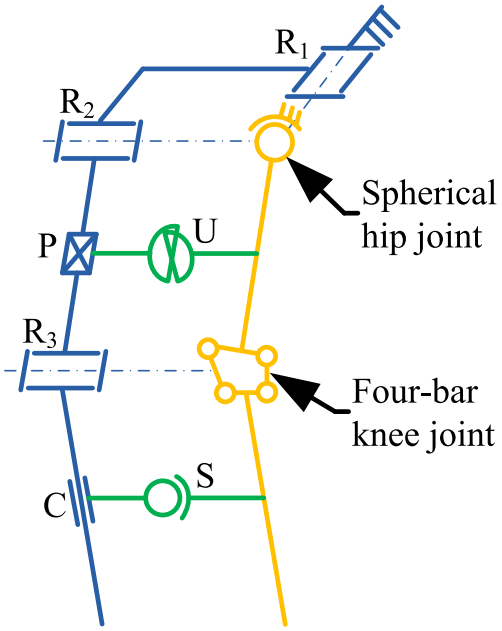

Fig. 4 Kinematic chain of the self-adapting exoskeleton

as self-tracing exoskeletons. In [28], a general configuration synthesis approach of the self-adapting lower-limb exoskeletons was proposed, in which the passive joints are introduced into the rigid human-robot connections (i.e., the rigid connective parts are replaced by passive human-robot connective joints), to eliminate the hyperstaticity of the human-robot closed chains. Using this method, a self-adapting exoskeleton mechanism for three-DOF lower-limb gait training is presented and shown in Fig. 4. In this mechanism, R_i indicates the active revolute joint, whereas P, S, U, and C denote the passive prismatic, spherical, universal and cylindrical joints, respectively. As the exoskeleton mechanism is connected to a human leg, a three-DOF human-robot closed chain is formed, and the number of corresponding DOFs can be verified as follows:

$$F = \sum_{i=1}^{n} f_i - dl = 15 - 12 = 3 \tag{1}$$

where n denotes the number of joints included in human-robot closed chain, f_i is the DOFs permitted by joint ith, $l = 2$ denotes the number of the independent loops included in human-robot closed chain, and d denotes the order of the motion space, in which the human-robot closed chain is intended to function (for a spatial chain $d = 6$).

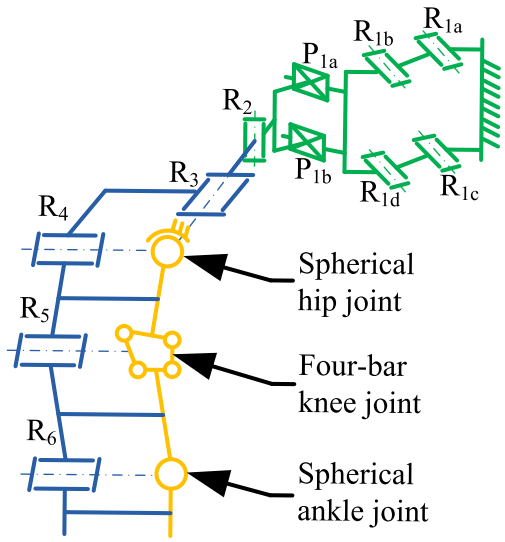

Fig. 3 Kinematic chain of the ALEX exoskeleton [23]

2.2 Structure Design of the Exoskeleton Mechanism

According to the kinematic configuration proposed in Fig. 4, a self-adapting lower-limb exoskeleton mechanism was designed, and the CAD schematic and the mechanical prototype are shown in Fig. 5. In this exoskeleton mechanical prototype, R_{11} and R_{21}, R_{12} and R_{22}, R_{13} and R_{23} denote the right and left AD/AB hip joints, the right and left FL/EX hip joints, as well as the right and left FL/EX knee joints, respectively; P_{11} and U_{11}, C_{11} and S_{11} indicate the upper and lower human-robot connective joints on the right, whereas P_{21} and U_{21}, C_{21} and S_{21} denote the upper and lower human-robot connective joints on the left. Moreover, in this study, all of the joints in the exoskeleton mechanism are passive, i.e., the human hip and the knee joints are active in human-robot closed chain, and the exoskeleton mechanism is driven by human legs during the p-HRI force measurement process. Accordingly, the exoskeleton prototype should possess the features of having a compact structure, being lightweight and being easy to

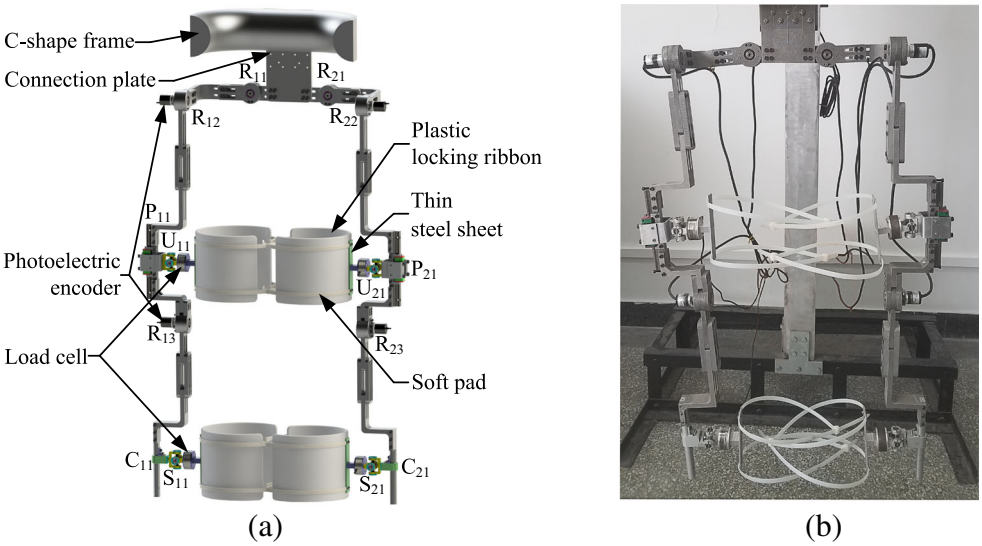

Fig. 5 The CAD schematic (**a**) and the mechanical prototype (**b**) of the exoskeleton mechanism

wear. To compare the p-HRI force between the exoskeleton mechanisms with or without connective joints, suitable load detecting cells should be selected and well installed, in particular, the same human-robot connective position should be ensured (i.e., for the detection cases of the p-HRI force with or without connective joints, the connective position should not change). With these considerations, the mechanical prototype of the exoskeleton mechanism was developed, which features the following design characteristics:

(1) The high-intensity aluminum parts with small cross-sections were utilized in mechanical prototype to reduce the weight of the lower-limb exoskeleton mechanism.
(2) The part lengths of the exoskeleton prototype could be adjusted to match the body parameter changes of the wearers.
(3) The connective cuff contains a bar of thin steel sheet, a piece of soft pad, and two plastic locking ribbons, which exhibits light weight and can fasten the human leg tightly.
(4) Six photoelectric encoders were mounted at joint R_{11}, R_{12}, R_{13}, R_{21}, R_{22} and R_{23}, with them, the rotation angles of the aforementioned joints could be detected directly.
(5) Two load cells are installed at the connective interfaces between the upper/lower cuffs and the joints U_{11}/S_{11}, respectively, by which the p-HRI forces between the right leg and the exoskeleton mechanism are measured.
(6) To achieve structural symmetry and thus to not affect the detection results, two parts with the same structures and weights as the two load cells are mounted at the connective interfaces between the upper/lower cuffs and the joints U_{21}/S_{21} in the left branch of the exoskeleton mechanism, respectively.
(7) The human-robot connective joints P_{11}, U_{11}, C_{11}, S_{11} and P_{21}, U_{21}, C_{21}, S_{21} are equipped with removable sheets and pins, which allow for the wearer to lock or unlock the connective joints quickly without detaching the human legs from the exoskeleton mechanism, and thus, the same human-robot connective position could be maintained.

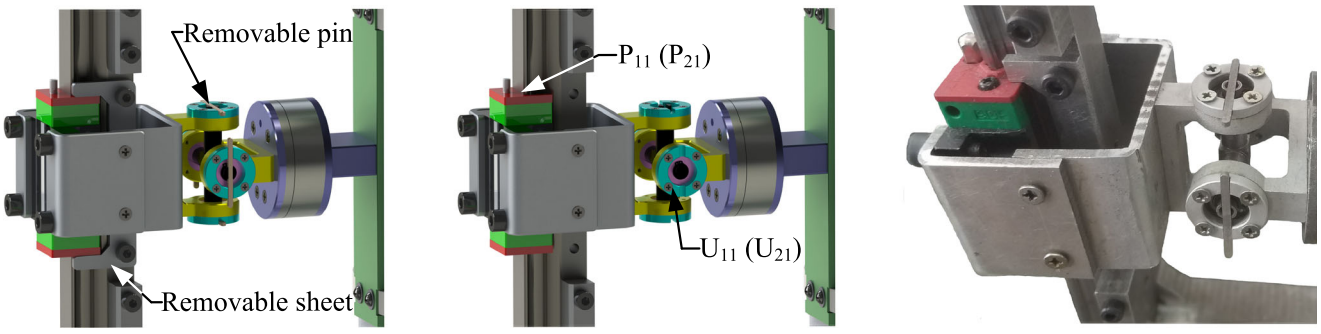

Fig. 6 The CAD models (**a** locked, **b** unlocked) and prototypes (**c**) of joints P_{11} (P_{21}), U_{11} (U_{21})

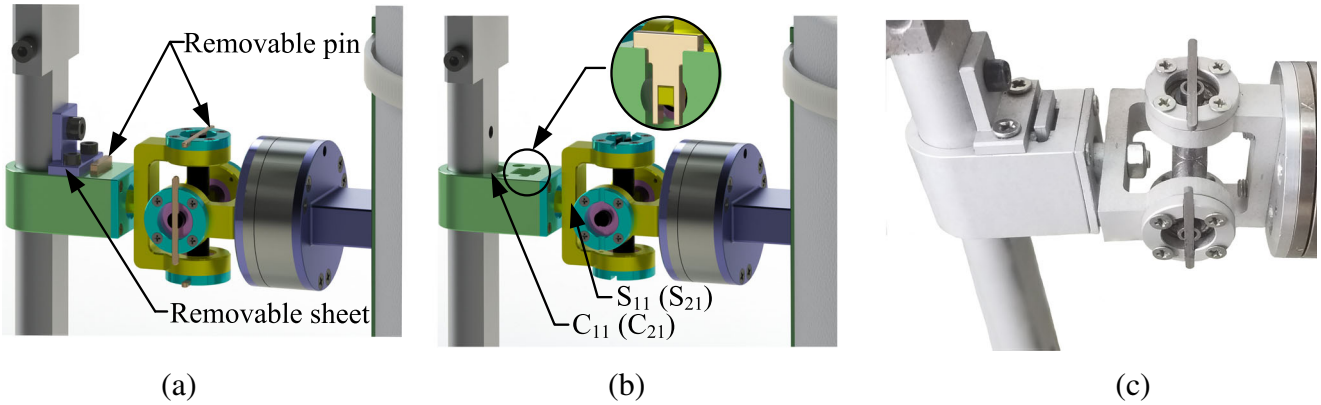

Fig. 7 The CAD models (**a** locked, **b** unlocked) and prototypes (**c**) of joints C_{11} (C_{21}), S_{11} (S_{21})

The CAD models and the prototypes of joints P_{11} (P_{21}) and U_{11} (U_{21}) are shown in Fig. 6, and the locked and unlocked situations of the two joints are illustrated in Fig. 6a and b, respectively. In the structure design of the joint P_1 (P_{21}), two pieces of removable sheets are used to lock or unlock the joint. In the structure design of the joint U_{11} (U_{21}), each revolute joint is equipped with two removable pins at the two ends of the joint, with which the revolute joint could be locked or unlocked quickly.

The structure deigns and the prototypes of joints C_{11} (C_{21}) and S_{11} (S_{21}) are shown in Fig. 7. In joint C_{11} (C_{21}), a flat is cut on the cylindrical surface of the exoskeleton's calf part, and a removable sheet as shown in Fig. 7a is used to lock or unlock the joint C_{11} (C_{21}). Joint S_{11} (S_{21}) is composed of a universal joint and a horizontal revolute joint; the corresponding axes of which could be locked or unlocked by removable pins.

2.3 Development of the p-HRI Force Measurement System

The p-HRI force measurement system was developed and shown in Fig. 8, which is mainly composed of the exoskeleton mechanism, a supporting frame, a treadmill and a data acquisition subsystem. In this measurement system, the exoskeleton mechanism is connected to a C-shape frame through a connection plate; meanwhile, the connection plate is connected to a backplane, which is fixed on the supporting frame by two parallel installed slide-ways. Such a design concept allows for the whole exoskeleton mechanism to move along with the human waist in a horizontal direction, while the wearer walks on the treadmill and drive the exoskeleton mechanism synchronously. In the data acquisition sub-system, the photoelectric encoders (TRD-MB2048SS-2 M) and the six-axis force/torque sensors (ATI

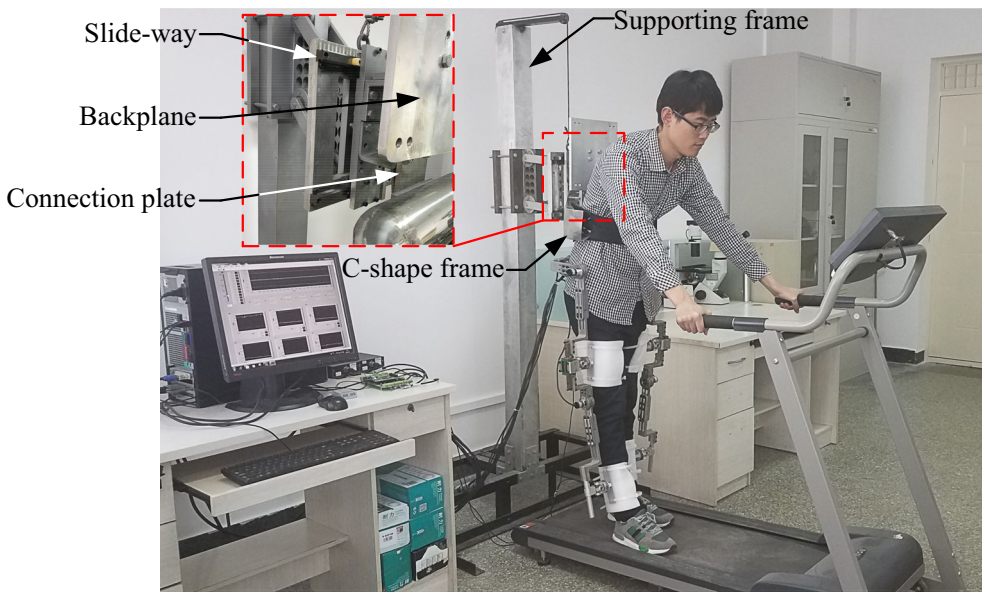

Fig. 8 The p-HRI force measurement system of the lower-limb exoskeleton mechanism

Mini45-SI-145-5) are utilized to detect the rotation angles and the p-HRI forces of the exoskeleton mechanism, respectively.

3 P-HRI Force Measurement and Analysis of the Exoskeleton Mechanism

In this section, the p-HRI force feature of the self-adapting lower-limb exoskeleton mechanism is investigated. Two kinds of motion modes, i.e., the gait mode and the static mode, of the human-robot closed chain are addressed, and the influences of the kinematic structure design (with or without human-robot connective joints) on the exoskeleton mechanism's p-HRI forces are analyzed according to the data detected by the six-axis force/torque sensors.

3.1 P-HRI Force Measurement of the Gait Mode

For the gait mode detection, two movement situations (i.e., the connective joints are locked and unlocked) of the human-robot closed chain are considered, respectively, and the p-HRI forces are detected by the upper and lower six-axis force/torque sensors, while the exoskeleton mechanism moves along with the human legs walking on a treadmill. The p-HRI force measurement of the gait mode is mainly carried out through the following procedures:

(1) Human-robot connection: a wearer stands naturally on a stationary treadmill, the waist, the thighs and the calves of whom are connected tightly with the lower-limb exoskeleton mechanism through the C-shape case and the connective cuffs, respectively, and all of the human-robot connective joints are locked by the removable sheets and pins.
(2) P-HRI force measurement (the connective joints are locked): the p-HRI forces are detected, while the exoskeleton mechanism moves along with the wearer walking on the treadmill with the speed of 8 km/h. To ensure the accuracy of the measurement, the p-HRI forces during six continuous gait cycles are collected for data acquisition after the motion state of the human-robot closed chain is stable.
(3) P-HRI force measurement (the connective joints are unlocked): the same data acquisition process performed as (2) is carried out for the p-HRI force measurement of the human-robot closed chain during six continuous gait cycles (the speed of the treadmill remains 8 km/h); the only difference is that all of the sheets and pins in locked connective joints are removed.

The angle trajectories of joints R_{11}, R_{l2}, and R_{13}, collected by the photoelectric encoders during the six continuous gait cycles, are shown in Fig. 9. Here, the green solid lines and the blue dotted lines indicate the human-robot closed chain with the locked and unlocked connective joints, respectively. From Fig. 9a–c, it can be seen that the angle trajectories of joints R_{11}, R_{l2}, and R_{13} change periodically, which indicates that the human-robot closed chain moves stably during the six continuous gait cycles.

The p-HRI force and torque components, i.e., $f_{(\mathrm{up/lo})x}$, $f_{(\mathrm{up/lo})y}$, $f_{(\mathrm{up/lo})z}$, $t_{(\mathrm{up/lo})x}$, $t_{(\mathrm{up/lo})y}$, and $t_{(\mathrm{up/lo})z}$, of the human-robot closed chain at the upper and lower connective interfaces, collected during six continuous gait cycles, are shown in Figs. 10 and 11 (the green solid lines and the blue dotted lines refer to the cases of the human-robot closed chain with locked and unlocked connective joints, respectively); it can be seen that both the force and torque components change periodically and thus are valid and suitable for influence analysis of the structure design on the exoskeleton mechanism's p-HRI force performance. Moreover, the force norm and the torque norm of the p-HRI could be calculated, based on the collected component data shown in Figs. 10 and 11, respectively, using the following equations:

$$F_{\mathrm{up/lo}} = \sqrt{f^2_{(\mathrm{up/lo})x} + f^2_{(\mathrm{up/lo})y} + f^2_{(\mathrm{up/lo})z}} \tag{2}$$

$$T_{\mathrm{up/lo}} = \sqrt{t^2_{(\mathrm{up/lo})x} + t^2_{(\mathrm{up/lo})y} + t^2_{(\mathrm{up/lo})z}} \tag{3}$$

where F_{up}, T_{up} and F_{lo}, T_{lo} indicate the norms of the force and torque components at the upper and lower connective interfaces, respectively.

The norm curves of the p-HRI force and torque components at the upper and lower connective interfaces are calculated and shown in Figs. 12a–b and 13a–b, respectively, based on which the following summaries could be obtained:

(1) The value ranges of F_{up1} and F_{up2}, T_{up1} and T_{up2}, F_{lo1} and F_{lo2}, and T_{lo1} and T_{lo2} are given as $F_{\mathrm{up1}}\in$(0.403 14.779)N and $F_{\mathrm{up2}}\in$(4.694 20.784)N, $T_{\mathrm{up1}}\in$(0.025 1.011)Nm and $T_{\mathrm{up2}}\in$(0.510 1.949)Nm, $F_{\mathrm{lo1}}\in$(0.520 14.513)N and $F_{\mathrm{lo2}}\in$(3.142 20.678)N, and $T_{\mathrm{lo1}}\in$(0.005 0.299)Nm and $T_{\mathrm{lo2}}\in$(0.098 0.595)Nm, respectively, indicating that the norms of the p-HRI force and torque components at the upper and lower connective interfaces are obviously decreased in magnitudes as the locked connective joints are replaced by the unlocked ones.
(2) The maximum values of F_{up1} and F_{up2}, T_{up1} and T_{up2}, F_{lo1} and F_{lo2},and T_{lo1} and T_{lo2} are given as $F_{\mathrm{mup1}} = 14.779$ N and $F_{\mathrm{mup2}} = 20.784$ N, $T_{\mathrm{mup1}} = 1.011$ Nm and $T_{\mathrm{mup2}} = 1.949$ Nm, $F_{\mathrm{mlo1}} = 14.513$ N and $F_{\mathrm{mlo2}} = 20.678$ N, and $T_{\mathrm{mlo1}} = 0.299$ Nm and $T_{\mathrm{mlo2}} = 0.595$ Nm, indicating that as the locked connective joints in human-robot closed chain are unlocked, the decreased levels of the maximum values of the norms of the p-HRI force and torque components at

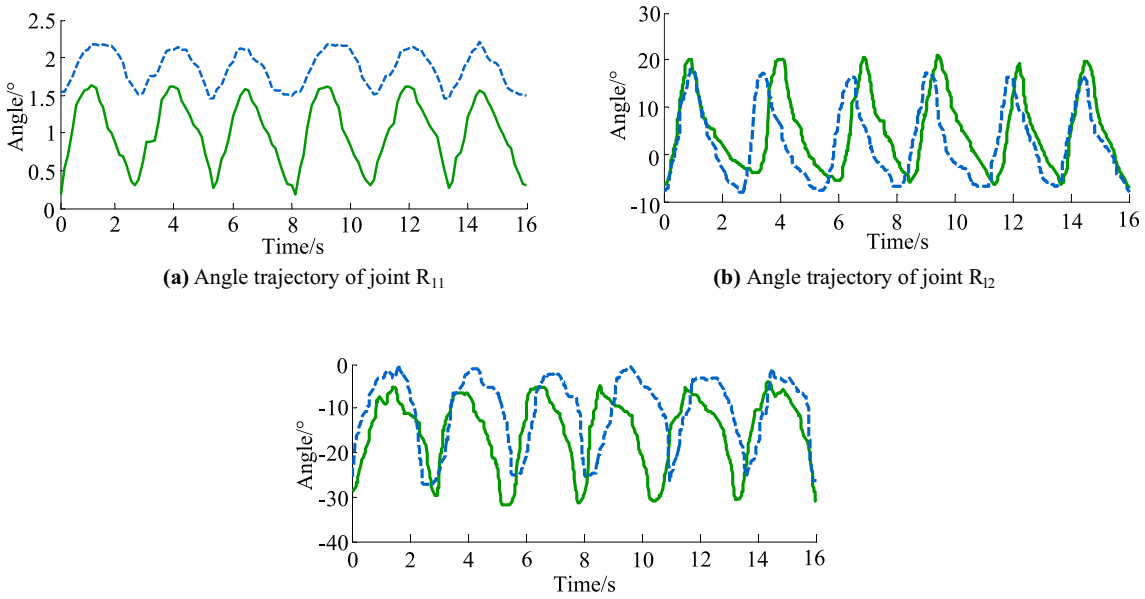

(a) Angle trajectory of joint R_{11}

(b) Angle trajectory of joint R_{l2}

(c) Angle trajectory of joint R_{13}

Fig. 9 The angle trajectories of joints R_{11}, R_{l2} and R_{13}

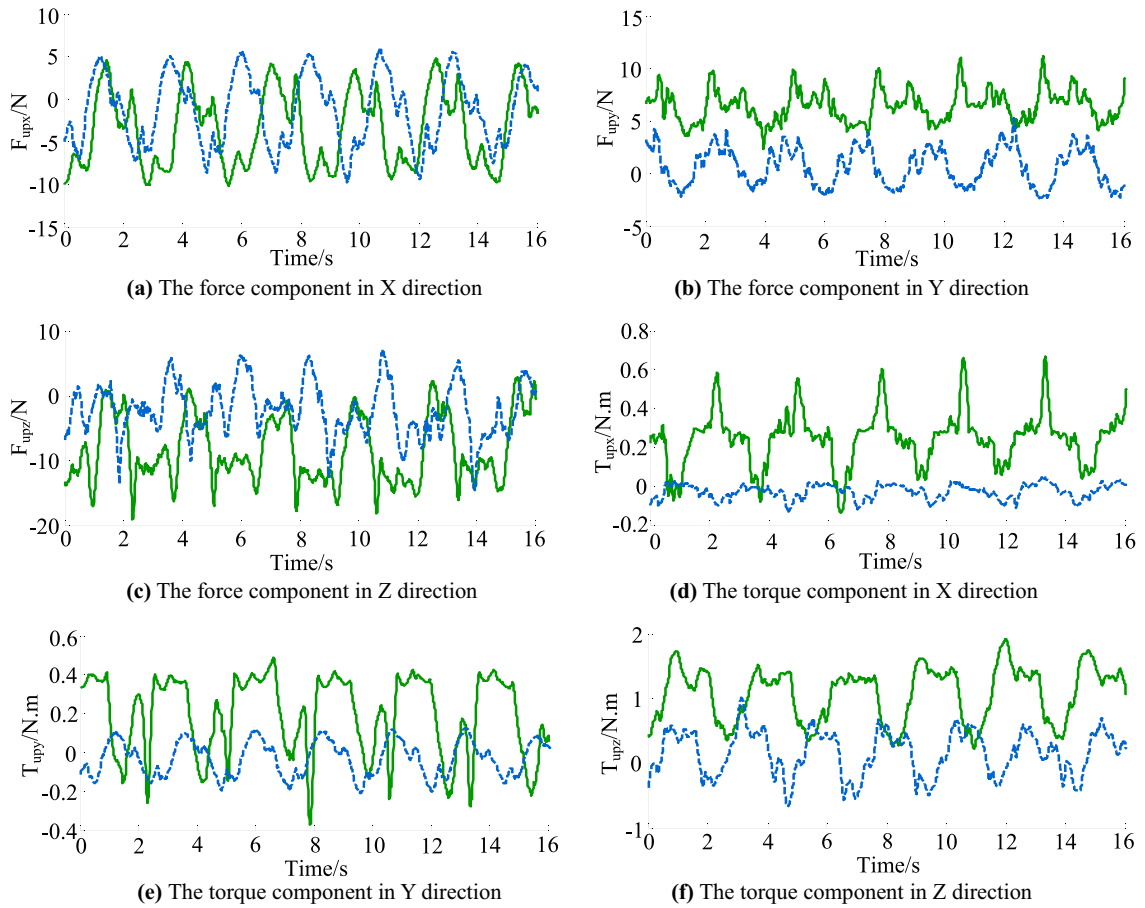

(a) The force component in X direction

(b) The force component in Y direction

(c) The force component in Z direction

(d) The torque component in X direction

(e) The torque component in Y direction

(f) The torque component in Z direction

Fig. 10 The p-HRI forces at the upper connective interface

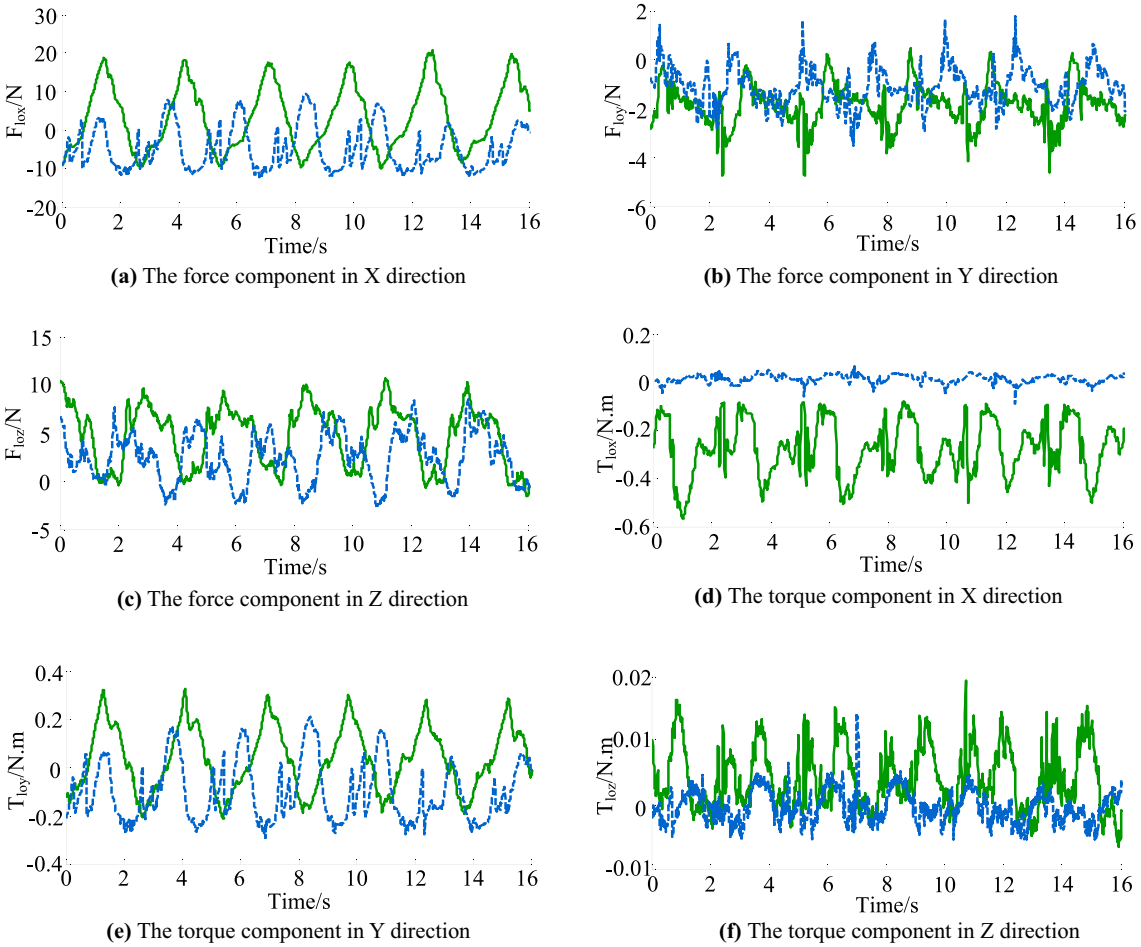

(a) The force component in X direction

(b) The force component in Y direction

(c) The force component in Z direction

(d) The torque component in X direction

(e) The torque component in Y direction

(f) The torque component in Z direction

Fig. 11 The p-HRI forces at the lower connective interface

the upper and lower connective interfaces may reach up to 28.89%, 48.13% and 29.81%, 49.75%, respectively.

(3) Finally, according to summaries (1) and (2), as well as the features of the value curves shown in Figs. 12a–b and 13a–b, it could be summarized that for gait mode, the p-HRI forces in human-robot closed chain can be reduced greatly by the unlocked connective joints, thus the proposed self-adapting lower-limb exoskeleton mechanism can improve the comfort of the p-HRI effectively.

3.2 P-HRI Force Measurement of the Static Mode

For the static mode detection, the p-HRI forces at the upper and lower connective interfaces of the human-robot closed chain, corresponding to six static configurations as shown in Figs. 14a–f and, with the locked and unlocked connective joints, are detected respectively. In addition, the width, length and height of each grid shown in Fig. 14a–f equal 5 cm, 10 cm, and 10 cm, respectively. To begin with, the wearer

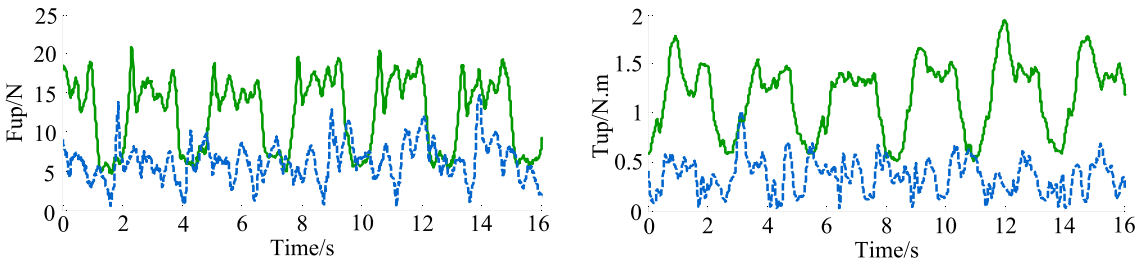

(a) The norm of the force components

(b) The norm of the torque components

Fig. 12 The norms of the p-HRI forces at the upper connective interface

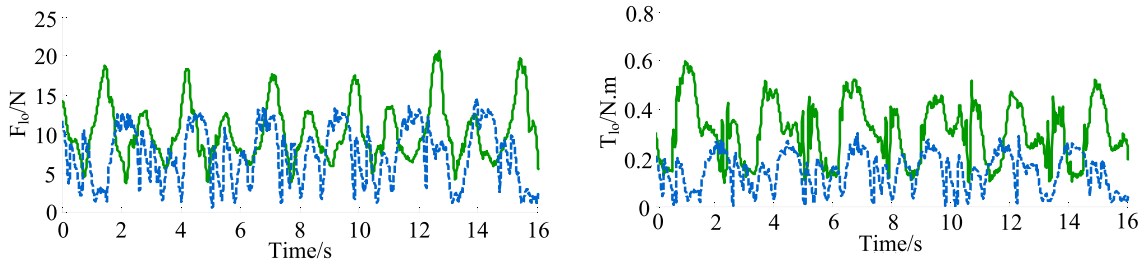

(a) The norm of the force components

(b) The norm of the torque components

Fig. 13 The norms of the p-HRI forces at the lower connective interface

stands naturally on the ground, the waist, thighs and calves of whom are tightly connected to the lower-limb exoskeleton mechanism, and all of the human-robot connective joints are locked by the removable sheets and pins. Then, the p-HRI force measurement in each static configuration is carried out through the following two procedures:

(1) P-HRI force measurement (the connective joints are

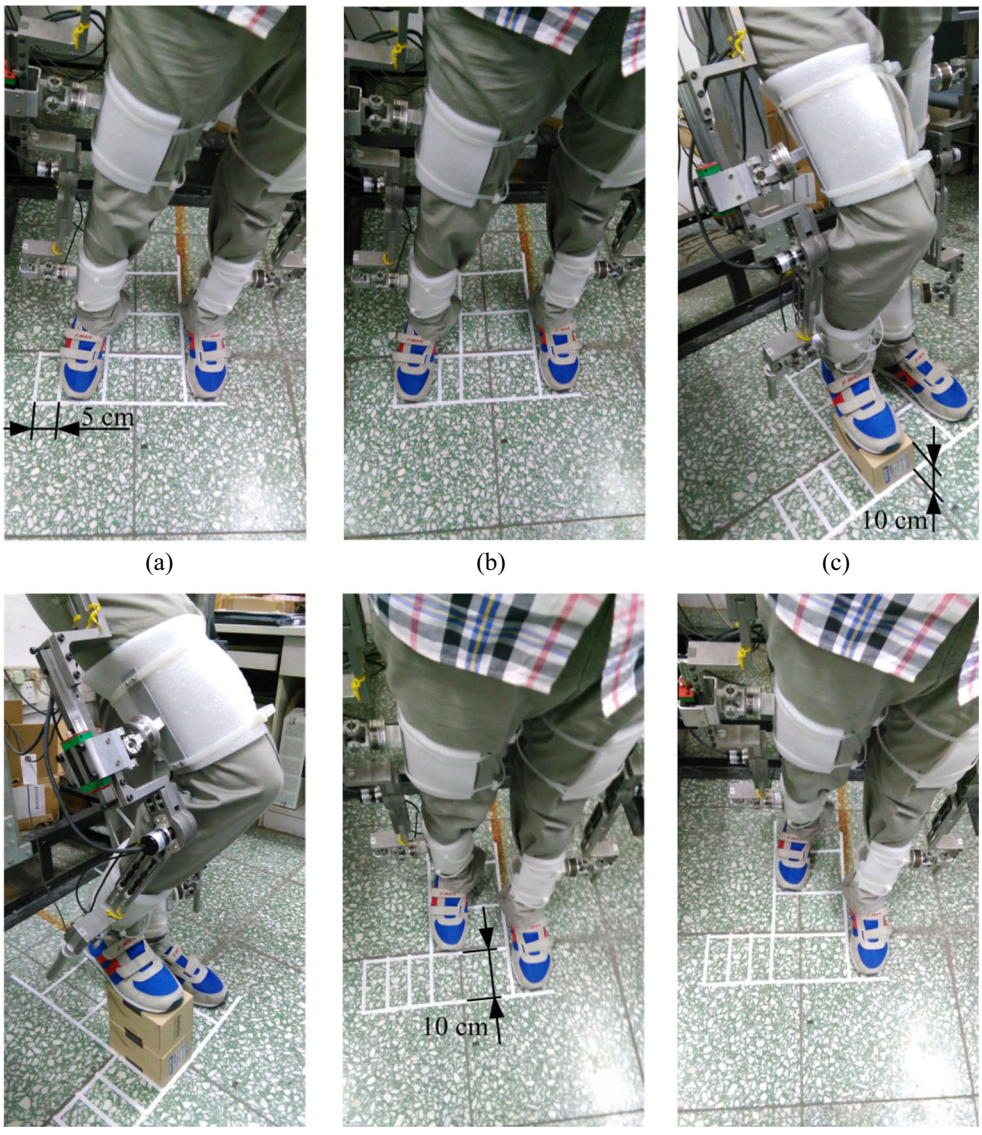

Fig. 14 Six static test configurations of the human-robot closed chain

Table 1 Norms of the force and torque components at six static test configurations

Configurations	Force norms (N)			Torque norms (Nm)		
(a)	Upper F/T sensor	locked	12.229	Upper F/T sensor	locked	0.605
		unlocked	4.364		unlocked	0.375
	Lower F/T sensor	locked	5.334	Lower F/T sensor	locked	0.215
		unlocked	3.862		unlocked	0.103
(b)	Upper F/T sensor	locked	14.487	Upper F/T sensor	locked	0.823
		unlocked	5.651		unlocked	0.580
	Lower F/T sensor	locked	11.233	Lower F/T sensor	locked	0.420
		unlocked	7.673		unlocked	0.196
(c)	Upper F/T sensor	locked	15.773	Upper F/T sensor	locked	0.405
		unlocked	9.854		unlocked	0.176
	Lower F/T sensor	locked	10.259	Lower F/T sensor	locked	0.406
		unlocked	8.451		unlocked	0.158
(d)	Upper F/T sensor	locked	26.810	Upper F/T sensor	locked	0.539
		unlocked	17.024		unlocked	0.347
	Lower F/T sensor	locked	15.428	Lower F/T sensor	locked	0.585
		unlocked	9.920		unlocked	0.266
(e)	Upper F/T sensor	locked	9.714	Upper F/T sensor	locked	0.757
		unlocked	7.378		unlocked	0.281
	Lower F/T sensor	locked	13.652	Lower F/T sensor	locked	0.321
		unlocked	10.627		unlocked	0.252
(f)	Upper F/T sensor	locked	16.582	Upper F/T sensor	locked	0.920
		unlocked	8.741		unlocked	0.482
	Lower F/T sensor	locked	17.634	Lower F/T sensor	locked	0.415
		unlocked	14.261		unlocked	0.328

locked): the right branch of the human-robot closed chain is moved by the human right leg to the test configuration, and then it is kept still there until the situation of the human-robot closed chain is stable. Subsequently, the p-HRI forces at the upper and lower connective interfaces are collected through the six-axes force/torque sensors. To ensure the accuracy of the data detection, the test duration is 10 s, and 1000 data points of each force/torque component are collected (the sampling frequency of the load cell is 100 Hz).

(2) P-HRI force measurement (the connective joints are unlocked): the same data acquisition process performed in (1) is carried out; the only difference is that all of the sheets and pins in locked connective joints are removed. To ensure consistency of the detection data, the test duration is also 10 s, and 1000 data points of each force/torque component are collected.

To perform an influence analysis of the kinematic structure design on the lower-limb exoskeleton mechanism's static-mode p-HRI force performance, the norms of the p-HRI force and torque components in six test configurations are calculated and listed in Table 1. Here, the means of the 1000 collected data points of each force/torque component are utilized in the norm calculations to improve the accuracy of the data.

In accordance with the values of the force norm and the torque norm given in Table 1, it can be seen that in the same static test configuration, both the force norm and the torque norm at the upper and lower connective interfaces of the human-robot closed chain are reduced to some extent as the locked connective joints are replaced by the unlocked ones. For the pairs of comparative test configurations, i.e., (a) and (b), (c) and (d), as well as (e) and (f), the force and torque norms corresponding to the former test configuration are smaller than those corresponding to the latter test configuration, under the situations in which the connective joints are locked and unlocked. Finally, it could be summarized that for the static mode, the unlocked connective joints can decrease the p-HRI forces at the human-robot interfaces and thus improve the p-HRI comfort of the proposed self-adapting lower-limb exoskeleton mechanism.

3.3 Discussion

Axis misalignment is a crucial problem in kinematic designs of wearable exoskeletons, and it should be well

dealt with to eliminate the hyperstaticity of the human-robot closed chains, and thus to decrease the uncontrollable hyperstatic forces at the human-robot interfaces; otherwise, the undesired force will be entirely unloaded on human's skin, soft issue and joint, and then causing harm to human. To implement this purpose, a kinematically compatible design has been considered in recent years, and two main synthesis methods of the exoskeleton kinematic configurations, including the self-tracing and the self-adapting approaches, have been presented. While different synthesis strategies were utilized, the two approaches were proposed on the same design principle that additional passive joints (or passive DOFs) are introduced into the exoskeleton mechanisms to avoid the over-actuation of the human-robot closed chains. The influence evaluation of the compatible design on a wearable exoskeleton's p-HRI performance is another important issue, which allows the designer to judge the satisfactoriness of the designed exoskeleton configuration. The novelty of this work is the proposal of a novel self-adapting kinematic configuration of the lower-limb exoskeleton mechanism for three-DOF gait training; by replacing the rigid connective parts that are used previous lower-limb exoskeletons with additional joints, the limited sliding and angular misalignments between the robotic and the human lower-limb, i.e., the undesired interactional loads in the human-robot chains, can be reduced. Based on this design concept, a p-HRI force measurement system was specially developed, and the influence of the compatible design on the exoskeleton mechanism's p-HRI force feature under both gait and static modes was analyzed by detecting the forces/torques at the upper and lower human-robot interfaces via the six-axis force/torque sensors. The results show that for gait and static detection modes, the p-HRI forces in human-robot closed chains could be reduced significantly. However, it should be highlighted that, due to the effect of the gravity of the exoskeleton mechanism in the static detection mode, as well as the effects of the gravity and the inertia of the human leg and the exoskeleton mechanism in the gait detection mode, the difference between the p-HRI forces/torques tested with locked and unlocked connective joints is not the value of the uncontrollable hyperstatic force/torque. For determining the values of the uncontrollable hyperstatic forces, the gravity and the inertia effects should be removed from the human-robot closed chains, which will be addressed in our future work. Moreover, the aesthetics, the stiffness and the concept of ergonomics will be considered carefully and improved effectively in our future prototype design. In any case, according to the results obtained in this study, it can be seen that the p-HRI forces decreased greatly with the additional human-robot connective joints, and thus, the compatible design of the lower-limb exoskeleton mechanism is effective.

4 Conclusion and Future Work

A p-HRI force measurement system is developed to analyze the influence of a compatible design on the lower-limb exoskeleton mechanism, which is composed of the designed exoskeleton mechanism with a self-adapting kinematic configuration, six photoelectric sensors for the angle detection of the hip and the knee joints of the exoskeleton mechanism, four six-axis force/torque sensors for detecting the p-HRI forces at the upper and lower human-robot connective interfaces, a treadmill, and a data acquisition sub-system. Specially, human-robot connective joints equipped with removable sheets and pins are designed, which ensure the wearer to lock or unlock the joints quickly without detaching the human legs from the exoskeleton mechanism.

The p-HRI forces of the human-robot closed chain, during six continuous gait cycles and in six static configurations, are detected, and the influence of the self-adapting design on the lower-limb exoskeleton mechanism's p-HRI force performance is analyzed. The results indicate that the compatible design of the lower-limb exoskeleton mechanism is effective, and the human-robot connective joints can significantly reduce the p-HRI forces in both the gait mode and static mode of the exoskeleton mechanism; thus, it is applied to human lower-limb gait training.

Future work will focus on the control system design, the exoskeleton prototype development, and the p-HRI force detection and interactional force characteristic evaluation of the exoskeleton prototype for the case in which the human-robot closed chain is moved by the lower-limb exoskeleton prototype.

Acknowledgements This work was supported by the National Natural Science Foundation of China under Grants No. 51675008 and No. 51705007, the Beijing Natural Science Foundation under Grants No. 3171001 and No. 17 L20019. Natural Science Foundation of Beijing Education Committee (No. KM201810005015) and China Postdoctoral Science Foundation (2018 T110017).

Compliance with Ethical Standards

Conflict of Interest We declare that we have no conflict of interest.

References

1. Hidler, J., Wisman, W., Neckel, N.: Kinematic trajectories while walking within the Lokomat robotic gait-orthosis. Clin. Biomech. **23**(10), 1251–1259 (2008)

2. Zanotto, D., Stegall, P., Agrawal, S. K.: ALEX III: A novel robotic platform with 12 DOFs for human gait training. In: IEEE International Conference on Robotics and Automation. Proceedings, pp. 3914–3919. IEEE, Germany (2013)
3. Veneman, J.F., Kruidhof, R., Hekman, E.E.G., Ekkelenkamp, R., Asseldonk, E.H.F.V., Kooij, H.V.D.: Design and evaluation of the LOPES exoskeleton robot for interactive gait rehabilitation. IEEE Trans. Neural Syst. Rehabil. Eng. **15**(3), 379–386 (2007)
4. Prange, G.B., Jannink, M.J.A., Groothuis-Oudshoorn, C.G.M., Hermens, H.J., Ijzerman, M.J.: Systematic review of the effect of robot-aided therapy on recovery of the hemiparetic arm after stroke. J. Rehabil. Res. Dev. **43**(2), 171–183 (2006)
5. Kwakkel, G., Kollen, B.J., Krebs, H.I.: Effects of robot-assisted therapy on upper limb recovery after stroke: a systematic review. Neurorehabil. Neural Repair. **22**(2), 111–121 (2008)
6. Gilliaux, M., Lejeune, T., Detrembleur, C., Sapin, J., Dehez, B., Selves, C., Stoquart, G.: A robotic device as a sensitive quantitative tool to assess upper limb impairments in stroke patients: a preliminary prospective cohort study. J. Rehabil. Med. **44**(3), 210–217 (2012)
7. Schiele, A., Helm, F.C.T.V.D.: Kinematic design to improve ergonomics in human robot interaction. IEEE Trans. Neural Syst. Rehabil. Eng. **14**(4), 456–469 (2006)
8. Schiele, A.: Ergonomics of exoskeletons objective performance metrics. In: world haptics-third joint Eurohaptics conference and symposium on haptic interfaces for virtual environment and teleoperator systems. pp. 103-108. IEEE, Salt Lake City (2009)
9. Stienen, A.H.A., Hekman, E.E.G., Helm, F.C.T.V.D., Prange, G.B., Jannink, M.J.A., Aalsma, A.M.M., Kooij, H.V.D.: DAMPACE: dynamic force- coordination trainer for the upper extremities. In: IEEE 10th International Conference on Rehabilitation Robotics. Proceedings, pp. 820–826. IEEE, Noordwijk (2007)
10. Nef, T., Guidali, M., Riener, R.: ARMinIII-arm therapy exoskeleton with an ergonomic shoulder actuation. Appl. Bionics Biomech. **6**(2), 127–142 (2009)
11. Celebi, B., Yalcin, M., Patoglu, V.: ASSISTON-KNEE: A self-aligning knee exoskeleton. In: IEEE/RSJ International Conference on Intelligent Robots and Systems. Proceedings, pp. 996–1002. Tokyo (2013)
12. Vitiello, N., Lenzi, T., Roccella, S., Rossi, S.M.M.D., Cattin, E., Giovacchini, F., Vecchi, F., Carrozza, M.C.: NEUROExos: a powered elbow exoskeleton for physical rehabilitation. IEEE T. Robot. **29**(1), 220–235 (2013)
13. Wu, Q., Wang, X., Chen, B., Wu, H.: Development of an RBFN-based neural-fuzzy adaptive control strategy for an upper limb rehabilitation exoskeleton. Mechatronics. **53**, 85–94 (2018)
14. Lee, Y., Kim, Y., Lee, J., Lee, M., Choi, B., Kim, J., Park, Y., Choi, J.: Biomechanical design of a novel flexible exoskeleton for lower extremities. IEEE-ASME T. Mech. 1–1 (2017)
15. Otten, A., Voort, C., Stienen, A., Aarts, R., Asseldonk, E., Kooij, H.: LIMPACT: a hydraulically powered self-aligning upper limb exoskeleton. IEEE-ASME T. Mech. **20**(5), 1–14 (2015)
16. Malosio, M., Pedrocchi, N., Vicentini, F., Tosatti, L.M.: Analysis of elbow-joints misalignment in upper-limb exoskeleton. In: 2011 IEEE International Conference on Rehabilitation Robotics. Proceedings, pp. 1–6. IEEE, Zurich (2011)
17. Dehez, B., Sapin, J.: ShouldeRO, An alignment-free two-DOF rehabilitation robot for the shoulder complex. In: 2011 IEEE International Conference on Rehabilitation Robotics. Proceedings, pp. 141–148. IEEE, Zurich (2011)
18. Galinski, D., Sapin, J., Dehez, B.: Optimal design of an alignment-free two-dof rehabilitation robot for the shoulder complex. In, IEEE International Conference on Rehabilitation Robotics. Seattle (2013)
19. Bartenbach, V., Wyss, D., Seuret, D., Riener, R.: A lower limb exoskeleton research platform to investigate human-robot interaction. IEEE International Conference on Rehabilitation Robotics. IEEE, In (2015)
20. Olivier, J., Bouri, M., Ortlieb, A., Bleuler, H., Clavel, R.: Development of an assistive motorized hip orthosis: Kinematics analysis and mechanical design. In: 2013 IEEE International Conference on Rehabilitation Robotics. Proceedings, pp. 1–5. IEEE, Washington (2013)
21. Stienen, A.H.A., Hekman, E.E.G., Helm, F.C.T.V.D., Kooij, H.V.D.: Self-aligning exoskeleton axes through decoupling of joint rotations and translations. IEEE T. Robot. **25**(3), 628–633 (2009)
22. Sergi, F., Accoto, D., Tagliamonte, N.L., Carpino, G., Pathiyil, L., Guglielmelli, E.: A systematic graph-based method for the kinematic synthesis of non-anthropomorphic wearable robots. In: 2010 IEEE International Conference on Robotics, Automation and Mechatronics. Proceedings, pp. 100–105. IEEE, Singapore (2010)
23. Jarrasse, N., Morel, G.: Connecting a human limb to an exoskeleton. IEEE T. Robot. **28**(3), 697–709 (2013)
24. Meuleman, J., Asseldonk, E., Oort, G., Rietman, H., Kooij, H.: LOPES II: design and evaluation of an admittance controlled gait training robot with shadow-leg approach. IEEE T. Neur. Sys. Reh. **24**(3), 352–363 (2015)
25. Mao, Y., Jin, X., Dutta, G., Scholz, J., Agrawal, S.: Human movement training with a cable driven ARm EXoskeleton (CAREX). IEEE T. Neur. Sys. Reh. **23**(1), 84 (2015)
26. Cui, X., Chen, W., Jin, X., Agrawal, S.: Design of a 7-DOF cable-driven arm exoskeleton (CAREX-7) and a controller for dexterous motion training or assistance. IEEE-ASME T. Mech. **22**(1), 1–1 (2016)
27. Jin, X., Cui, X., Agrawal, S.: Design of a cable-driven active leg exoskeleton (C-ALEX) and gait training experiments with human subjucts. In: 2015 IEEE International Conference on Robotics and Automation (ICRA), pp. 5578–5583. IEEE, Seattle (2015)
28. Li, J., Zhang, Z., Tao, C., Ji, R.: Structure design of lower limb exoskeletons for gait training. Chin. J. Mech. Eng. **28**(5), 878–887 (2015)
29. Li, J., Zhang, Z., Tao, C., Ji, R.: A number synthesis method of the self-adapting upper-limb rehabilitation exoskeletons. Int. J. Adv. Robot. Syst. **14**(3), 1–14 (2017)
30. Schiele, A., Visentin, G.: The ESA human arm exoskeleton for space robotics telepresence. In: 7th International Symposium on Artificial Intelligence, Robotics and Automation in Space. Proceedings. pp. 326–331. IEEE, Nara (2003)
31. Banala, S.K., Kim, S.H., Agrawal, S.K., Scholz, J.P.: Robot assisted gait training with active leg exoskeleton (ALEX). IEEE Trans. Neural Syst. Rehabil. Eng. **17**(1), 2–8 (2009)
32. Walsh, C.J., Endo, K., Herr, H.: A quasi-passive leg exoskeleton for load-carrying augmentation. Int. J. Humanoid Robot. **4**(3), 487–506 (2007)
33. Rossi, S.M.M.D., Vitiello, N., Lenzi, T., Ronsse, R., Koopman, B., Persichetti, A., Vecchi, F., Ijspeert, A.J., Kooij, H.V.D., Carrozza, M.C.: Sensing pressure distribution on a lower-limb exoskeleton physical human-machine interface. Sensors. **11**, 207–227 (2011)
34. Rathore, A., Wilcox, M., Ramirez, D.Z.M., Loureiro, R., Carlson, T.: Quantifying the human-robot interaction forces between a lower limb exoskeleton and healthy users. In: Proceedings of the 38th Annual International Conference of the IEEE Engineering in Medicine and Biology Society. pp. 586–589. IEEE, Orlando (2016)

35. Duque, J.T., Ugalde, R.C., Kilicarslan, A., Venkatakrishnan, A., Soto, R., Vidal, J.L.C.: Real-time strap pressure sensor system for powered exoskeletons. Sensors. **15**, 4550–4563 (2015)
36. Zanotto, D., Akiyama, Y., Stegall, P., Agrawal, S.: Knee joint misalignment in exoskeletons for the lower extremities: effects on user's gait. IEEE T. Robot. **31**(4), 978–987 (2015)
37. Schiele, A.: An explicit model to predict and interpret constraint force creation in pHRI with exoskeletons. In: proceedings of IEEE international conference on robotics and automation. pp. 1324-1330. IEEE. Pasadena. (2008)
38. Schiele, A.: Ergonomics of exoskeletons: Objective performance metrics. In: Proceedings of the Third Joint Eurohaptics Conference and Symposium on Haptic Interfaces for Virtual Environment and Tele-operator Systems. pp. 103–108. Salt Lake City (2009)
39. Schiele, A., Helmb, F.C.T.V.D.: Influence of attachment pressure and kinematic configuration on pHRI with wearable robots. Appl. Bionics Biomech. **6**(2), 157–173 (2009)
40. Jarrasse, N., Tagliabue, M., Robertson, J., Maiza, A., Crocher, V., Roby-Brami, A., Morel, G.: A methodology to quantify alterations in human upper limb movement during co-manipulation with an exoskeleton. IEEE Trans. Neural Syst. Rehabil. Eng. **18**(4), 389–397 (2010)
41. Wang, H.: Anatomy of the human system. Fudan University Press, Shanghai, China (2008)
42. Cenciarini, M., Dollar, A.M.: Biomechanical considerations in the design of lower limb exoskeletons. In: 2011 IEEE international conference on rehabilitation robotics. IEEE. Zurich. (2011)
43. Cai, V.A.D., Bidaud, P., Hayward, V.: Self-adjusting, isostatic exoskeleton for the human knee joint. In: Proceedings of the Annual International Conference of the IEEE Engineering in Medicine and Biology Society. pp. 612–618. IEEE, Boston (2011)
44. Celebi, B., Yalcin, M., Patoglu, V.: AssistON- Knee: a self-aligning knee exoskeleton. In: IEEE/RSJ International Conference on Intelligent Robots and Systems (2013)
45. Radcliffe, C.W.: Four-bar linkage prosthetic knee mechanisms: kinematics, alignment and prescription criteria. Prosthetics Orthot. Int. **8**(18), 159–173 (1994)
46. Yamaguchi, G.T., Zajac, F.E.: A planar model of the knee joint to characterize the knee extensor mechanism. J. Biomech. **22**(1), 1–10 (1989)
47. Bapat, G., Sujatha, S.: A method for optimal synthesis of a biomimetic four-bar linkage knee joint for a knee-ankle-foot orthosis, J. Biomech. **32**, 20–28 (2017)
48. Chen, G., Qi, P., Guo, Z., Yu, H.: Mechanical design and evaluation of a compact portable knee–ankle–foot robot for gait rehabilitation. Mech. & Mach. Theory. **103**, 51–64 (2016)
49. Xu, L., Wang, D.H., Fu, Q., Yuan, G., Hu, L.Z.: A novel four-bar linkage prosthetic knee based on magnetorheological effect: principle, structure, simulation and control. Smart Mater. Struct. **25**(11), 115007 (2016)

Pulisher's Note Springer Nature remains neutral with regard to jurisdictional claims in published maps and institutional affiliations

Jianfeng Li received the Ph.D. degree in mechanical engineering from Beihang University, Beijing, China, in 1999. After a postdoctor from Tsinghua University, he came back to Beijing University of Technology in 2001 and was elected as a professor in 2008. His research interests include theory of parallel mechanism, wearable exoskeleton, external fixator and rehabilitation robotics.

Shiping Zuo was born in Liaoning of China in 1994. He received the bachelor degree in mechanical and electrical engineering from Tianjin Polytechnic University, Tianjin, China, in 2016. He is the M.E. student in mechanical engineering from Beijing University of Technology, Beijing, China, at present. His research interests include parallel mechanism, exoskeleton mechanism and rehabilitation robotics.

Chenghui Xu received the M.E. degree in mechanical engineering from Beijing University of Technology, Beijing, China, in 2017. His research interests include wearable exoskeleton technology.

Leiyu Zhang received the M.E. degree (2009) and the Ph.D. degree (2016) in mechanical engineering from Beihang University, Beijing, China. He is now a lecturer in the College of Mechanical and Electrical Engineering in the Beijing University of Technology. His research interests include rehabilitation exoskeletons, configuration analysis, physical Human-Robot interaction and movement analysis.

Mingjie Dong received the Ph.D. degree in Mechatronics from Beihang University, Beijing, China, in 2018, and now he is a faculty member in the College of Mechanical Engineering and Applied Electronics Technology in Beijing University of Technology. His research interests include sensor calibration, sensor fusion and intelligent control of rehabilitation robotics.

Chunjing Tao received the Ph.D. degree in Institute of Electrical Engineering in Chinese Academy of Sciences, Beijing, China, in 2007. She is in Beijing Key Laboratory of Aged Functional Rehabilitation Assisted Technology and she is a master student tutor of Beijing University of Technology and University of Shanghai for Science and Technology, at present. Her research interests include rehabilitation equipment design and wearable exoskeleton technology.

Run Ji received the bachelor degree in Prosthetic Orthopaedic Engineering from Capital Medical University, Beijing, China, in 2008. He is an assistant researcher in National Research Center for Rehabilitation Technical Aids. His research interests include rehabilitation equipment design and wearable exoskeleton technology.